170 (2022) 207371

Contents lists available at ScienceDirect

Micro and Nanostructures

journal homepage: www.journals.elsevier.com/micro-and-nanostructures

Nonlinear optical characteristics of thermodynamic effects- and electric field-triggered Mathieu quantum dot

M.K. Bahar *, P. Başer

Department of Physics, Faculty of Science, Sivas Cumhuriyet University, 58140, Sivas, Turkey

ARTICLE INFO

Keywords:
Total refractive index
Total absorption coefficients
Mathieu quantum dot
Hydrogenic impurity
Hydrostatic pressure
External electric field

ABSTRACT

In this work, the total refractive index (TRICs) and total absorption coefficients (TACs) of a spherical quantum dot with the Mathieu potential encompassement, generated by using $In_xGa_{1-x}As/GaAs$ heterostructure, and including hydrogenic impurity in its center, under the influence of the temperature, hydrostatic pressure and external electric field are investigated. The compact density matrix formalism and the iterative method are employed to compute the nonlinear optical features. The relevant eigenvalue equation of the Mathieu quantum dot (MQD) is solved by constructing a tridiagonal matrix formalism, within the effective mass approach. As well as the response of TRICs and TACs to external parameters, the alterations concerning structure parameters such as doping concentration and restriction width are also examined. To the best of our knowledge, the external influences and structural parameters on the optical specifications of MQD containing the central impurity are theoretically taken into consideration, for the first time, in the present work. Determining the optimality of optical properties arising from structural and external parameter changes is crucial in terms of providing a theoretical basis for the experimental production and practical use of MQD.

1. Introduction

In paralel with the development of well-experienced and current crystal growth techniques, the manufacturation of low-dimensional structures that constrain the movement of carriers is possible [1,2]. Quantum dots are still of great interest theoretically and experimentally, as they display outstanding results in terms of optical and electronic properties compared to other low-dimensional systems [3]. Moreover, these structures are very advantageous in optoelectronic technology as they have a very wide and tunable absorption spectrum ranging from the ultraviolet to the visible spectrum wavelength. Therefore, the devices including quantum dot are effectively utilized in many areas such as medical and military imaging [4], various electronic and optoelectronic applications [5–9]. Quantum dots can be evaluated as artificial atoms, and their geometrical modifications enables to readily tune the band gap of system. Absorption and radiation features can be determined by size or by size-independent considering material structure, for the alloy semiconductor $In_xGa_{1-x}As/GaAs$ quantum dots [10]. One of the most striking features of quantum dots is their adjustability geometrically. Determining the form of the encompassing potential is essential in formulating any theory of quantum dots. Some experimental studies suggest that the optimal quantum dot profiles to encompass electrons should be of the well-like [11]. Because of this experimental prediction, this work focuses on the quantum dot profile, which exhibits a well-type, that is, a parabolic-type encompassement. The Mathieu potential provides such a motivation. Also, the Mathieu potential has both depth (V_0)

* Corresponding author.
E-mail addresses: mussiv58@gmail.com (M.K. Bahar), pbaser34@gmail.com (P. Başer).

https://doi.org/10.1016/j.micrna.2022.207371
Received 6 July 2022; Received in revised form 15 August 2022; Accepted 15 August 2022
Available online 26 August 2022

and width parameter (η). In this way, the results arising from the width and depth of the quantum dot to be produced experimentally are examined theoretically in a more realistic way and presented to the use of experimental researchers. Moreover, such a quantum dot can be easily produced by advanced experimental techniques [12]. The Mathieu potential is a periodically recurring potential for wider spatial boundaries, which is an important model for possible applications of multiple quantum nanostructures. On the other hand, there are exact analytical solutions of the Mathieu potential, and thanks to these solutions, the statistical properties of the Mathieu quantum dot can also be examined. In fact, relativistic solutions for the Mathieu potential have also been explored. The Mathieu potential is an important potential in the materials physics area. All these realities provide a strong motivation for us to consider the quantum dot (MQD) modeled by the Mathieu potential. The optical properties of MQD which has aforementioned important advantages provide a different motivation factor due to their importance, and it is realized by us, for the first time, to the best of our knowledge. Many researches have been performed on parabolic quantum dots [13–17]. In this study, we investigate the nonlinear optical properties of MQD, including a hydrogenic impurity in its center, formed by $In_xGa_{1-x}As/GaAs$, which in turn has never been considered before, to the best of our knowledge. The Mathieu potential is taken into consideration in the literature to be able to elucidate the physical properties of solid-state materials and in their surface state calculations. Some studies have performed photoemission computations for the free electron by regarding the Mathieu potential [18]. In this manner, it is shown that the exact solutions of the one-dimensional Schrödinger equation involving the Mathieu potential are given by combined Heun functions [19]. In addition, in some theoretical studies, considering the Dirac equation involving scalar and vector potentials, the relativistic wave equation with Mathieu potential is solved within the spin symmetry [20].

In this work, the preference of $In_xGa_{1-x}As/GaAs$ heterostructure is because this structure allows remarkable electronic, optical and optoelectronical applications. $In_xGa_{1-x}As$ has the essential function in a photodetector application with high-speed and high-sensitivity, which makes it important for fiber optic telecommunications [21]. Only lattice-matched low-dimensional heterostructures or ones including pseudomorphic strain-layer, on suitable substrate, by employing conventional semiconductors (GaAlAs/GaAs) preferred in laser applications, can be obtained. Therefore, the limited wavelengths in these structures preclude further advanced heterostructure designs [22]. Whereas, heterostructures obtained by using InGaAs have a wider wavelength range than lattice-matched semiconductors, and if there is strain in these structures, modification of the energy band structure reduces greatly the current densities [22]. The band gap energy of $In_xGa_{1-x}As$ (for x=0.47) at room temperature is 0.75 eV, which is advantageous for fiberoptic communication. Also, the low effective mass of $In_xGa_{1-x}As$ results in high mobility. Device efficiency increases as high mobility reduces series resistance. Mobility and band gap can be changed depending on the In concentration in InGaAs, which is very useful for tuning the respective device performances [23]. In summary, $In_xGa_{1-x}As$ are semiconductors that provide important application possibilities for photodetectors, lasers, photovoltaics and transistors [24–26]. The above-mentioned advantages of $In_xGa_{1-x}As$ were sufficiently focused in considering the $In_xGa_{1-x}As/GaAs$ heterostructure in this work. These materials have many essential microelectronic applications such as high speed electron mobility transistors [27–30]. External factors such as the pressure and temperature exerted on semiconductors are substantial thermodynamic variables that provide an operational argument for tuning and optimizing their electronic and optical properties. Some special specifications such as hole energies, can be tuned systematically without the need to modificate the sample, thanks to the applied hydrostatic pressure, provided that structural phase transformations do not occur. The pressure and temperature alter the confinement effects of the particles and the energy gap of the material. It is seen that while the energy gap of the material increases as the pressure effect increases, it decreases as the temperature increases. For example, at room temperature, when increasing from $P = 5$ GPa to $P = 15$ GPa, the energy gap $E_g(In_{0.15}Ga_{0.75}As)$ increases from $E_g =$ 1.80eV to $E_g = 2.99$eV. Whereas, when the temperature is increased from $T = 0$K to $T = 300$K in the case of $P = 0$ GPa, $E_g(In_{0.15}Ga_{0.75}As)$ decreases from $E_g = 1.28$eV to $E_g = 1.21$eV. The pressure and temperature, because of these remarkable changes, modify the optical and electronic features of the material. There are many experimental and theoretical investigations probing the influences of the pressure and temperature on the electronic-optical features of III-V semiconductor compounds [31–36]. In order to design and optimize many optoelectronic devices exploiting these semiconductors and set the appropriate band gap, it is crucial to determine the operational character of the band gap change depending on pressure and temperature. The impression of factors such as the hydrostatic pressure and temperature in consideration of nonlinear optical properties of low-dimensional systems is particular. In the GaAs-$Ga_{1-x}Al_xAs$ asymmetric double quantum well, the change of nonlinear optical absorption and nonlinear optical rectifications with hydrostatic pressure as well as applied electric and magnetic fields have been examined, and it has been presented that nonlinear optical absorption can be altered depending on the pressure [37]. Also, it has been analyzed how to change the linear, nonlinear and total optical features of the AlGaAs/GaAs semi-parabolic quantum well in the presence of the temperature, hydrostatic pressure, and external magnetic field, and it has been observed that the TRIC amplitudes monotonically decrease as a result of increasing in the hydrostatic pressure [38]. In Ref. [38], it has also been determined that TRICs are strongly dependent on the temperature T. Because, the resonant peaks enhance and shift towards higher energy spectrum as the temperature increases. As expected, there are blatant results of the temperature and pressure effect on TACs. When the temperature is increased as $T = 0$K, $T = 200$K and $T = 400$K, while it is observed that the TACs amplitudes also rise, the changing as $P = 0$ kbar, $P = 50$ kbar and $P = 100$ kbar in the pressure leads to a reducing in TACs amplitudes [38]. The pressure and temperature affect other nonlinear optical features such as second-third harmonic generations (SHG-THG) and nonlinear optical rectification (NOR) as well as TACs and TRICs. When the influences of the magnetic field, hydrostatic pressure and temperature on the NOR and SHG in an asymmetric Gaussian quantum well are examined theoretically, it is confirmed that the hydrostatic pressure and temperature redshift the SHG resonant peaks, and the NOR resonant peaks decrease with increasing hydrostatic pressure and temperature [39]. In the SHG analysis of $GaAs/Ga_{1-x}Al_xAs$ asymmetric double semi-parabolic quantum well, it has been shown that while the resonant peaks shift to blue as the temperature increases, they shift to red because of increasing pressure [40].

Impurity states in low-dimensional systems have marked effects in semiconductor physics due to their spectacular modification

impacts on the electronic and optical properties of the system. These properties provide a very practical application in optoelectronic devices technology because they become tunable the radiation and conduction properties of the material. In addition to the impurity states, the energy spectrum of the systems can be changed significantly though the external electric field applied on the system. Many theoretical studies have been carried out to review the electric field effect on quantum dots with and without hydrogen impurities [41–44]. The motivation for such studies is that the electric field elicits the well-known quantum confinement Stark effect in the literature, which is characterized by a much more vivid redshift than the electron-hole binding energy. Both experimental and theoretical investigations that consider the results of the applied electric field on the encompassed carriers show that two substantial situations can arise simultaneously: One of them is the redshift of the excitonic absorption, and the another is the expansion that occurs in the quantum constrained Stark effect. As expected, when an electric field is applied, band bending occurs, creating an inclined band structure that changes blatantly the localization probability. Thus, the electron subband energy level reduces and the hole subband energy level escalates, which leads to a red shift of the excitonic absorption. The another effect is the increment in the energy of the electron-hole pair, and also the decrement in the Coulomb interaction between them, due to the mobility of electron and hole in contrary directions resulting from this bending, as result of the polarization of the exciton, which causes to a blue shift. Both of these observed effects are urgent consequences of the electric field applied to the structure. In a nutshell, the aforementioned single particle confinement and related interaction produce the anomalous excitonic Stark shift [45]. Tuning the subband transition is very important to control the optical behavior under the electric field, and therefore many studies have been done to analyze the impact of the electric field on the optical features of the system [46–48]. It has been shown that TRICs and TACs are significantly affected due to the applied electric field on the bound state localizations. In this context, it has been shown that for a given quantum dot size and incident photon intensity, the interband optical nonlinearity can be properly tuned by acting an external electric field [47]. In some studies, it has been observed that optical absorption increases with augmenting electric field in the case of impurity in the center of the quantum dot [48]. In studies investigating parallel and vertical electric field effects on SiGe prolate and oblate quantum dots, the redshifted nonlinear optical properties due to increasing electric field have been confirmed [49].

In our work, the remarkable influences of external electric field, hydrostatic pressure and temperature on the electronic and optical features of MQD with the centrally located impurity-containing have been determined. In this context, the present work provides important data for studies on new device designs thanks to determination of the functional F, P and T range, and these external variables can be employed as alternatives to each other in applications. The Mathieu potential, as mentioned before, is used to depict the physical properties of condensed materials, in surface state calculations, and the crystal potential from that the initial state wave function for the surface state is obtained [50]. Due to the possibility of experimentally generating this potential in a well-like structure within the magnification restriction, the determined theoretical results may be striking for practical applications. In this work, the effects of external parameters such as hydrostatic pressure, temperature and electric field as well as structural parameters and centrally-located hydrogenic impurity on electronic energies, TRICs and TACs are investigated. The results show that TRICs and TACs are sensitive to quantum dot's spatial restrictions and confinement. In this sensitivity, the external and structural parameters can be evaluated as alternatives to each other in consideration of situations such as resonant shifting and optimality. Also, the diversity of the variable number is crucial for device designs, and then with this motivation, the MQD's TRICs and TACs have been probed.

The article is promoted as follows: In Section II, the theoretical model considered in the study is elucidated. In Section III, the findings and comments are represented. In Section IV, the important results highlight.

2. Theoretical model

For a hydrogenic impurity at the center of MQD in the presence of the external electric field, hydrostatic pressure, and temperature, the Hamiltonian is furnished by

$$H = -\frac{\hbar^2\nabla^2}{2m^\star(P,T)} + V_{dot}(r) + |e|\xi r cos(\theta) - \frac{Ze^2}{4\pi\epsilon_0\epsilon(P,T)r} \tag{1}$$

with

$$m^\star(P,T) = \left[1 + E_P^\Gamma\left(\frac{2}{E_g^\Gamma(P,T)} + \frac{1}{E_g^\Gamma(P,T)+0.341}\right)\right]^{-1} m_0, \tag{2}$$

where m_0 is the free electron mass, $\epsilon(P, T)$ is the static dielectric constant as function of the pressure and temperature [53], stating as

$$\epsilon(P,T) = \begin{cases} 12.74exp\big(-1.67\times10^{-2}P\big)exp\big(9.4\times10^{-5}(T-75.6)\big), & \text{if } T \le 200K \\ 13.18exp\big(-1.73\times10^{-2}P\big)exp\big(20.4\times10^{-5}(T-300)\big), & \text{if } T > 200K. \end{cases} \tag{3}$$

Also, for GaAs(InGaAs), $E_g^\Gamma(P,T)$ including $E_P^\Gamma(P,T) = 7.51$eV is the energy gap as function of the pressure and temperature, in units of eV, and in the following form:

$$E_g^\Gamma(P,T) = E_g^0 + \alpha P - \beta T^2(T+c)^{-1}, \tag{4}$$

where, being $\alpha = 10.8\times10^{-2}$ eV/GPa($\alpha = 7.7\times10^{-2}$ eV/GPa) the pressure coefficient, $\beta = 5.405\times10^{-4}$ eV/K ($\beta = 4.19\times10^{-4}$ eV/K)

and $c = 204$K ($c = 271$K) temperature coefficients, respectively, for GaAs (and InAs), $E_g^0 = 1.52$eV($E_g^0 = 0.42$eV) is the energy gap when $P = 0$ GPa and $T = 0$K [53,54]. $E_g(P, T)$ may be stated for $Ga_xIn_{1-x}As$ depending on x (In-concentration), P and T as follows [54]:

$$E_g^{GaInAs}(P,T) = E_g^{GaAs}(P,T) + \left[E_g^{InAs}(P,T) - E_g^{InAs}(P,T)\right]x - 0.475x(1-x). \tag{5}$$

MQD depth (V_0) is given as function of the pressure and temperature in the following form [55,56]:

$$V_0(P,T) = \begin{cases} \left(E_g^{GaAs}(P,T) - E_g^{GaInAs}(P,T)\right) \times 0.7, & \text{if } r \geqslant R_{dot}(P) \\ 0, & \text{if } r < R_{dot}(P). \end{cases} \tag{6}$$

The quantum dot radius ($R_{dot}(P)$) should be modified due to the hydrostatic pressure as follows [57];

$$R_{dot}(P) = R(0)(1 - 3(S_{11} + 2S_{12})P)^{(1/3)} \tag{7}$$

with

$$\begin{array}{lcl} C_{11} & = & (8.34 + 3.56x)10, \\ C_{12} & = & (4.54 + 0.8x)10, \\ S_{11} & = & (C_{11} + C_{12})/((C_{11} - C_{12})(C_{11} + 2C_{12})\,), \\ S_{12} & = & -C_{12}/((C_{11} - C_{12})(C_{11} + 2C_{12})\,). \end{array} \tag{8}$$

In Eq. (1), ξ is the external electric field strength, θ is the angle between the electric field vector and radial distance vector. $V_{dot}(r)$ is MQD potential, expressing as

$$V_{dot}(r) = V_0(P,T)\left(sin^2(\eta r) - cos(\eta r)\right) \tag{9}$$

with the potential depth parameter V_0, the potential width parameter η. Since the angular solutions of the wave equation $H\psi(r, \theta, \varphi) = E\psi(r, \theta, \varphi)$ of the system are well-known as the spherical harmonics $Y_\ell^m(\theta, \varphi)$, it can be suggested as $\psi(r, \theta, \varphi) = R(r)Y_\ell^m(\theta, \varphi)$. Then, considering $R(r) = P(r)r^{-1}$, the radial Schrödinger equation is written in the following form:

$$\frac{d^2P(r)}{dr^2}\left[\frac{2m^\star(P,T)}{\hbar^2}\left(E - V_{eff}(r,P,T,\xi)\right)\right]P(r) = 0 \tag{10}$$

with

$$V_{eff}(r,P,T,\xi) = V_{dot}(r) + |e|\xi r - \frac{Ze^2}{4\pi\epsilon_0\epsilon(P,T)r} + \frac{\hbar^2}{2m^\star(P,T)}\frac{\ell(\ell+1)}{r^2}. \tag{11}$$

The Eq. (11) is solved though tridiagonal matrix method [58]. For detail, please refer [58].

The linear and nonlinear susceptibilities are procured though the density-matrix approach, they are expressed in closed analytical form as follows [59].

$$\epsilon_0\chi^{(1)}(\omega) = \frac{\sigma_\nu\left|M_{fi}\right|^2}{E_{21} - \hbar\omega - i\hbar\Gamma_{if}}, \tag{12}$$

$$\begin{array}{lcl} \epsilon_0\chi^{(3)}(\omega) & = & -\dfrac{\sigma_\nu\left|M_{fi}\right|^2\left|\widetilde{E}\right|^2}{E_{fi} - \hbar\omega - i\hbar\Gamma_{if}} \times \left[\dfrac{4\left|M_{fi}\right|^2}{\left(E_{fi} - \hbar\omega\right)^2 + \left(\hbar\Gamma_{if}\right)^2} - \right. \\ & & \left. \dfrac{\left(M_{ff} - M_{ii}\right)^2}{\left(E_{fi} - i\hbar\Gamma_{if}\right)\left(E_{fi} - \hbar\omega - i\hbar\Gamma_{if}\right)}\right] \end{array} \tag{13}$$

with σ_ν (the carrier density), $E_{i,f}$ (the initial (i) and final (f) energy state), M_{fi} (being f, i the final and initial state, respectively, the dipole matrix elements ensured using $M_{fi} = <f|\vec{r}|i>$), $\Gamma = 1/\tau$ is the relaxation rate for i, f states, ω is the incident photon energy, $\widetilde{E}$ is the electromagnetic field amplitude. Also, in computations of M_{if}, the following property of the spherical harmonics is taken into consideration [60],

$$cos\theta Y_{\ell m}(\theta,\varphi) = Q_{\ell-1,m}Y_{\ell-1,m}(\theta,\varphi) + Q_{\ell,m}Y_{\ell+1,m}(\theta,\varphi), \tag{14}$$

where

$$Q_{\ell,m} = \left[\frac{(\ell+1)^2 - m^2}{(2\ell+1)(2\ell+3)}\right]^{1/2}. \tag{15}$$

Considering Eq. (14) and Eq. (15), it is found that [60].

$$< n'\ell'm' \mid r\cos\theta \mid n\ell m >= \left(Q_{\ell-1,m}\delta_{\ell',\ell-1} + Q_{\ell,m}\delta_{\ell',\ell+1}\right) I'_{n\ell n'\ell'}\delta_{m',m}, \tag{16}$$

where

$$I'_{n\ell n'\ell'} = \int_0^{R_{dot}(P)} Q_{n\ell}Q_{n'\ell'}\,r dr. \tag{17}$$

The dipole matrix elements are procured though Eq. (16) by regarding $\triangle\,\ell = \pm 1$. The linear and the third-order nonlinear RICs are expressed as [59].

$$\frac{\Delta n^{(1)}(\omega)}{n_r} = \frac{\sigma_v |M_{fi}|^2}{2n_r^2\epsilon_0}\left[\frac{E_{fi}-\hbar\omega}{\left(E_{fi}-\hbar\omega\right)^2 + \left(\hbar\Gamma_{if}\right)^2}\right], \tag{18}$$

$$\begin{aligned}\frac{\Delta n^{(3)}(\omega,I)}{n_r} &= -\frac{\mu c|M_{fi}|^2}{4n_r^3\epsilon_0}\frac{\sigma_v I}{\left[\left(E_{fi}-\hbar\omega\right)^2 + \left(\hbar\Gamma_{if}\right)^2\right]^2} \\ &\times\left[4\left(E_{fi}-\hbar\omega\right)\left|M_{fi}\right|^2 - \frac{\left(M_{ff}-M_{ii}\right)^2}{\left(E_{fi}\right)^2 + \left(\hbar\Gamma_{if}\right)^2}\left\{\left(E_{fi}-\hbar\omega\right)\right.\right. \\ &\times\left.\left.\left[\left(E_{fi}\right)\left(E_{fi}-\hbar\omega\right) - \left(\hbar\Gamma_{if}\right)^2\right] - \left(\hbar\Gamma_{if}\right)^2\left(2\left(E_{fi}\right)-\hbar\omega\right)\right\}\right],\end{aligned} \tag{19}$$

where μ, c, and I are, respectively, the system permeability, the light speed in vacuum, and the incident optical intensity. The TRIC is presented by adding the linear and nonlinear contributions [59]:

$$\frac{\Delta n(\omega,I)}{n_r} = \frac{\Delta n^{(1)}(\omega)}{n_r} + \frac{\Delta n^{(3)}(\omega,I)}{n_r}. \tag{20}$$

The linear and the third-order nonlinear ACs are expressed as

$$\alpha^{(1)}(\omega) = \omega\sqrt{\frac{\mu}{\epsilon_r}}\,\frac{|M_{fi}|^2\sigma_v\hbar\Gamma_{if}}{\left(E_{fi}-\hbar\omega\right)^2 + \left(\hbar\Gamma_{if}\right)^2}, \tag{21}$$

$$\begin{aligned}\alpha^{(3)}(\omega,I) &= -2\omega\sqrt{\frac{\mu}{\epsilon_R}}\left(\frac{I}{\epsilon_0 n_r c}\right)\times\frac{|M_{fi}|^4\sigma_v\hbar\Gamma_{if}}{\left[\left(E_{fi}-\hbar\omega\right)^2 + \left(\hbar\Gamma_{if}\right)^2\right]^2}\left(1 - \frac{|M_{ff}-M_{ii}|^2}{|2M_{fi}|^2}\right. \\ &\times\left.\frac{\left(E_{fi}-\hbar\omega\right)^2 - \left(\hbar\Gamma_{if}\right)^2 + 2\left(E_{fi}\right)\left(E_{fi}-\hbar\omega\right)}{\left(E_{fi}\right)^2 + \left(\hbar\Gamma_{if}\right)^2}\right).\end{aligned} \tag{22}$$

The TAC is represented by adding the linear and nonlinear contributions [59]:

$$\alpha(\omega,I) = \alpha^{(1)}(\omega) + \alpha^{(3)}(\omega,I). \tag{23}$$

For detail, please refer [59,61]. It is important to note that the selection rules $\triangle\,\ell = \pm 1 (m = 0)$ are taken into consideration in the present work. In addition, some parameter values are considered as $m_{GaAs} = 0.067m_0$ (m_0 is mass of the free electron), $R_{dot}(P=0) = 6a_0$, $\epsilon_{GaAs} = 13.18$, $n_r = 3.2$ and $\tau = 0.2$ ps. In this case, the effective Rydberg energy and Bohr radius are computed as $R_y^* \cong 5.28$ meV and $a_0 = 103.7\,\mathring{A}$, respectively [51,52].

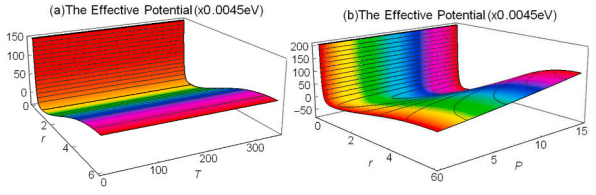

Fig. 1. The effective potential profile of the MQD system with $x = 0.15$, $\eta = 0.35/a_0$, $P = 3$ GPa and $F = 1$ kV/cm, (a) as function of the radial distance ($r(a_0)$) and temperature ($T(K)$), (b) as function of the radial distance ($r(a_0)$) and hydrostatic pressure ($P(GPa)$). Note:$\ell = 1$ and $m = 0$.

3. Result and discussions

The influences of the structure parameters such as the Mathieu potential width parameter (η) and $In-$ concentration (x) as well as the external effects such as the hydrostatic pressure, temperature and electric field on TRICs and TACs of $In_xGa_{1-x}As/GaAs$ spherical MQD are also taken into account. In this manner, the influences of different five parameters in the effective potential are probed. In Fig. 1, the profiles of the effective potential, including the MQD encompassement potential, are presented as function of the potential parameters and the radial distance (r). Panel $-$ a in Fig. 1 is for the temperature (T), panel $-$ b is for the hydrostatic pressure (P). In Fig. 2, the quantum dot potential is shown as function of radial distance, and with which panel $-$ a, panel $-$ b, panel $-$ c are, respectively, for the potential depth (V_0), MQD width (η), and electric field strength ξ. In Fig. 3a and c, the optical intensity effect on the TRICs of MQD, respectively, as $I = 0.05 \times 10^{10}$, 0.2×10^{10} and $0.3 \times 10^{10} W/m^2$, and the effect of electron density as $\sigma_\nu = 4 \times 10^{23}$, 6×10^{23}, and $8 \times 10^{23} m^{-3}$ are introduced for the incident photon energy. In Fig. 3b and d, the optical intensity effect on the TACs of MQD, respectively, as $I = 0.05 \times 10^{10}$, 0.1×10^{10} and $0.2 \times 10^{10} W/m^2$, and the effect of electron density as $\sigma_\nu = 4 \times 10^{23}$, 6×10^{23}, and $8 \times 10^{23} m^{-3}$ are represented for the incident photon energy. In Fig. 3a, the TRICs resonant amplitudes decrease due to the increment in nonlinear contribution based on the increasing optical intensity. Further increase in optical intensity, where $I = 0.3 \times 10^{10} W/m^2$, elicits unstable the TRICs character as it causes structural distortions in the quantum dot. Therefore, it can be said that the upper limit of the incoming optical density for the TRICs under the relevant conditions is around $I = 0.3 \times 10^{10} W/m^2$. As expected in Fig. 3b, it is monitored that the TACs resonant amplitudes decrease prominently because of the enhancement of I. Structural instabilities observed for $I = 0.3 \times 10^{10} W/m^2$ in the TRICs characteristic are emerged for $I = 0.2 \times 10^{10} W/m^2$ in consideration of the TACs. Thus, it can be said that for the TRICs and TACs, under the respective conditions, unstable states resulting from structural deterioration occur at different $I-$ values. These results, caused by the structural distortions observed in the properties of the TRICs and TACs, allow us to determine the maximum and optimal I for TRICs and TACs. In Fig. 3c and d, it is seen that the TRICs and TACs resonant peaks increase as the electron density increases, which is an expected case.

In Fig. 4, the TRICs and TACs characteristics are furnished for some temperature values as a function of the incident photon energy. The augmentation of the temperature has a slight impact on encompassement effects, and due to this slight effect, the bound state localizations hardly alter, as can be seen in Fig. 1a. This slight response is also reflected on the energy gaps between the subbands, and matrix elements. In this case, as can be seen in Fig. 4, it can be noted that the temperature change does not have remarkable effects on the TRICs and TACs characters.

In Fig. 5a and b, respectively, the TRICs and TACs of MQD are shown for some hydrostatic pressure values as $P = 0, 3, 9, 15$ GPa, as a function of the incident photon energy. The TRICs and TACs are impressed markedly from the change in hydrostatic pressure. As seen in Fig. 5a and b, the resonant frequency of TRICs and TACs shifts to lower range as hydrostatic pressure increases. As seen in Fig. 1b, the strength of the confinement effect increases dependently to enhancing the pressure, which causes to reduce the energy differences between the subbands of the MQD (See Fig. 5a, b insets). However, both the TRICs and TACs amplitudes decrease due to the reduction in matrix elements resulting from increasing the hydrostatic pressure (See Fig. 5a, b insets).

In Fig. 6a and b, the TRICs and TACs of MQD versus four different values of $In-$ concentration are presented for the incident photon energy. Increasing x, hence increasing potential depth (See Fig. 2a), causes a blueshifted the TRICs and TACs resonant frequencies (See Fig. 6). Because the increase in the potential depth as well as the narrowing of the potential width causes an increment in the energy gap between localizations, as can be seen in the insets of Fig. 6. The TRICs amplitudes decrease with increasing potential depth, due to matrix elements decrease as x increases, as shown in Fig. 6a inset. As seen in Fig. 6b, the augmentation of $In-$ concentration enhances the TACs amplitudes, in contrast to the behavior of the TRICs amplitudes. Although the augment of $In-$ concentration reduces the matrix elements, the increase in the TACs amplitudes emerges from the mathematical prepotency between linear-nonlinear contribution that makes up the TACs.

Fig. 7a and b shows the TRICs and TACs characteristics as a function of some values of the parameter η for the incident photon energy. Since the enhancement of η increases the encompassement effect (See Fig. 2b), the difference between the subband energies increases, as can be seen from the energy gap change in the insets given in Fig. 7, and thus blatant blueshifted resonant frequencies occur. Also, in Fig. 7a, it is seen that the TRICs amplitudes decrease as a result of decreasing matrix elements due to increasing η (See

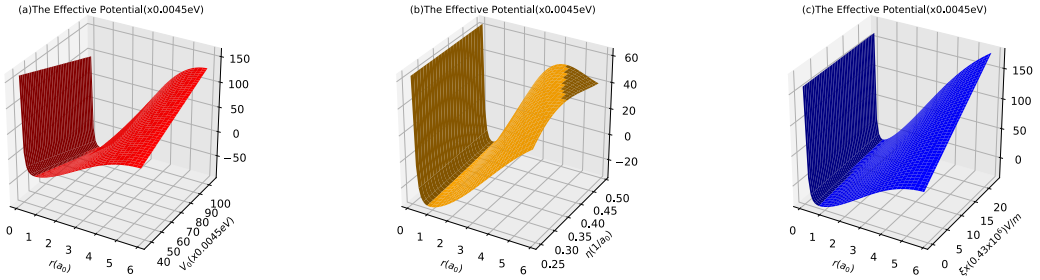

Fig. 2. The effective potential profile of the MQD system, (a) as function of the radial distance ($r(a_0)$) and potential depth (V_0) when $\eta = 0.35/a_0$, $T = 300$K, $P = 3$ GPa and $F = 1$ kV/cm, (b) as function of the radial distance ($r(a_0)$) and potential width ($\eta(a_0^{-1})$)) when $x = 0.15$, $T = 300$K, $P = 3$ GPa and $F = 1$ kV/cm, (c) as function of the radial distance ($r(a_0)$) and external electric field ($F(kV/cm)$) when $x = 0.15$, $\eta = 0.35/a_0$, $T = 300$K, $P = 3$ GPa. Note:$\ell = 1$ and $m = 0$.

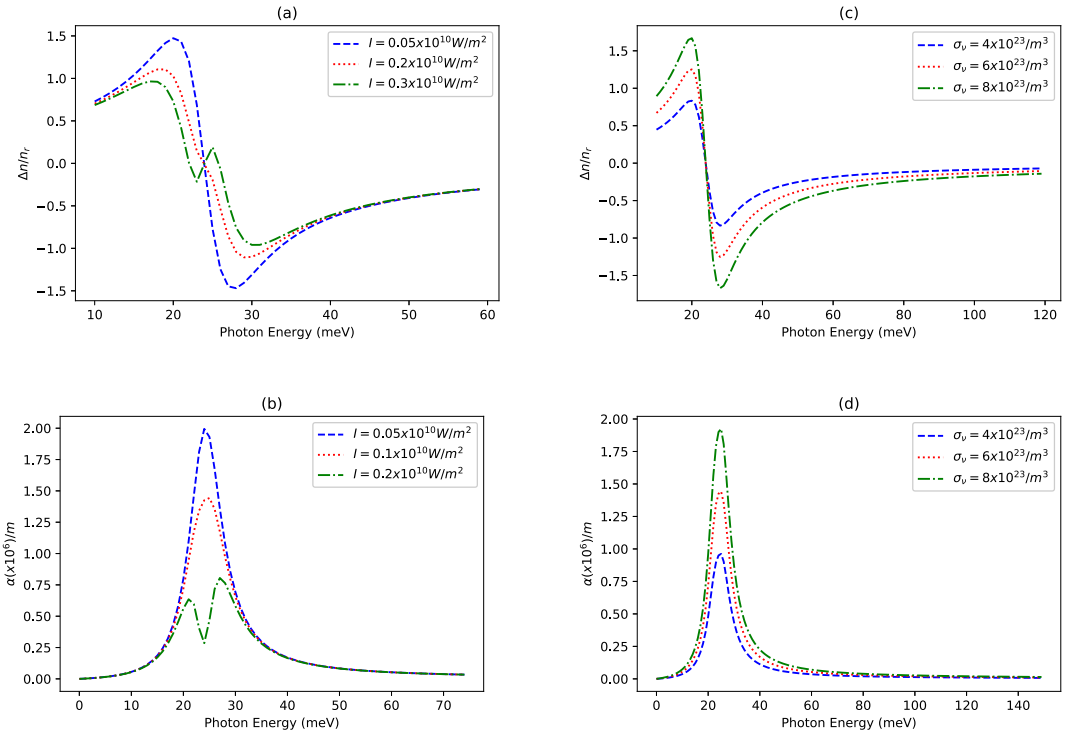

Fig. 3. For the MQD system with $x = 0.15$, $\eta = 0.35/a_0$, $T = 300$K, $P = 3$ GPa and $F = 1$ kV/cm, (a) the TRICs for $I = 0.05 - 0.2–0.3 \times 10^{10}$W/m^2 when $\sigma_v = 6 \times 10^{23}$m^{-3}, (b) the same of (a) but the TACs for $I = 0.05 - 0.1–0.2 \times 10^{10}$W/m^2, (c) the TRICs for $\sigma_v = 4–6–8 \times 10^{23}$m^{-3} when $I = 0.1 \times 10^{10}$W/m^2, (d) the same of (c) but the TACs.

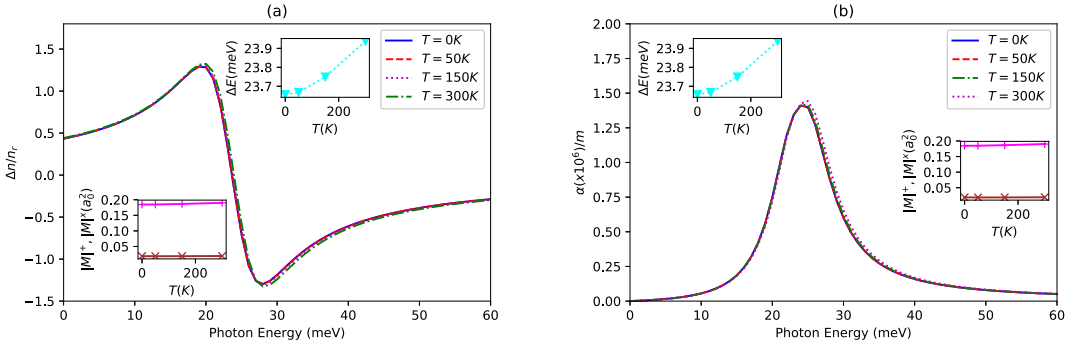

Fig. 4. When $I = 0.1 \times 10^{10}$W/m^2 and $\sigma_v = 6 \times 10^{23}$m^{-3}, the TRICs (panel (a)) and TACs (panel (b)) of the MQD system with $x = 0.15$, $\eta = 0.35/a_0$, $T = 0–50 - 150 - 300$K, $P = 3$ GPa and $\xi = 1$ kV/cm. The insets show the relevant energy differences and matrix elements, respectively, as $\Delta E = E_f - E_i$, $|M|^+ = |M_{if}|^2$, $|M|^x = |M_{ii} - M_{ff}|^2$.

Fig. 7a inset). It is great to mention that the blue-shifting considerations in the TRICs are also true in the TACs. However, the behavior of resonant amplitudes for the TACs as a result of increasing this parameter is the opposite of that for the TRICs. As seen in Fig. 7b, increasing the η parameter considerably escalates the TACs amplitudes. The reason for this is the precedence of the linear and nonlinear contribution to each other to form the absorption coefficients.

In Fig. 8a and b, the TRICs and TACs are presented for some external electric field values as a function of the incident photon energy. As seen in Fig. 8a, increasing ξ creates blueshifted resonant frequencies in terms of both the TRICs and TACs. Because, as it is clearly seen in Fig. 2c, when the electric field is acted in the growth direction, the trapping effect of the electron enhances, that is, the increasing electric field boosts the repulsion of the potential. As a more repulsive potential, as here, creates bound state localizations with greater energy gaps, an explicit blueshift occurs at the resonant frequencies of the TRICs and TACs This is clearly seen in Fig. 8a inset that presents the energy difference change depending on the electric field. Similarly, the TRICs amplitudes decrease due to the decrement in matrix elements as the external electric field strength increases (See Fig. 8a and its inset). The TACs have a similar character to the TRICs, due to altering electric field strength, except for the amplitudes. The behavior of the TACs resonant amplitudes

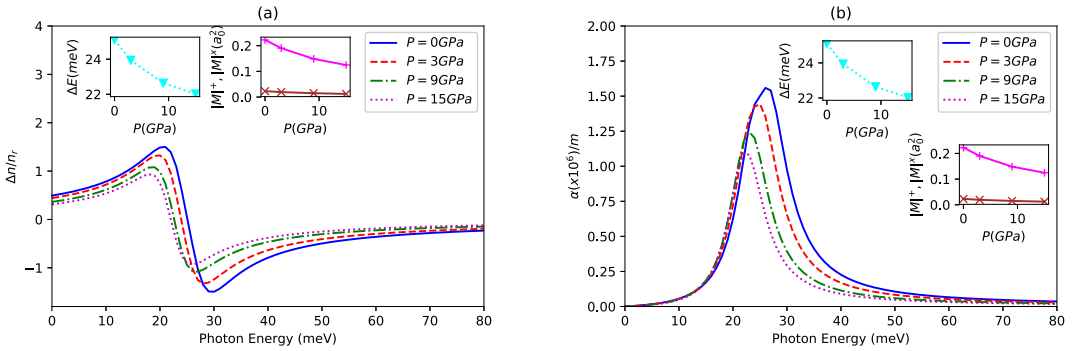

Fig. 5. When $I = 0.1 \times 10^{10}\mathrm{W/m^2}$ and $\sigma_\nu = 6 \times 10^{23}\mathrm{m^{-3}}$, the TRICs (panel (a)) and TACs (panel (b)) of the MQD system with $x = 0.15$, $\eta = 0.35/a_0$, $T = 300\mathrm{K}$, $P = 0\text{–}3 - 9 - 15$ GPa and $\xi = 1$ kV/cm. The insets show the relevant energy differences and matrix elements, respectively, as $\Delta E = E_f - E_i$, $|M|^+ = |M_{if}|^2$, $|M|^x = |M_{ii} - M_{ff}|^2$.

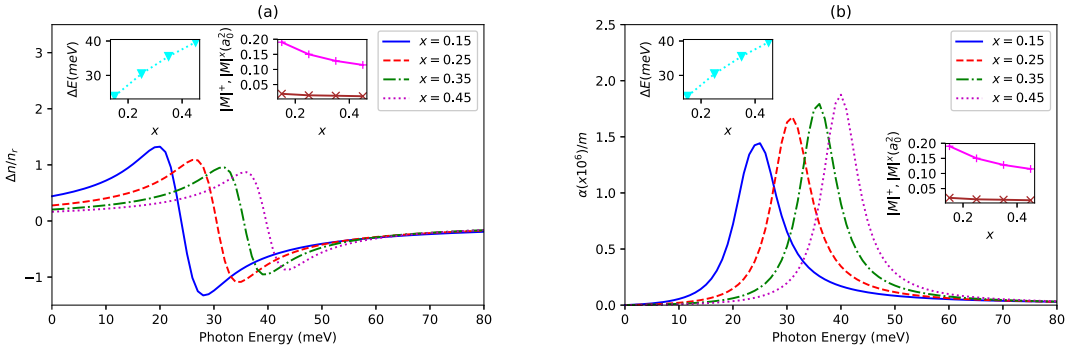

Fig. 6. When $I = 0.1 \times 10^{10}\mathrm{W/m^2}$ and $\sigma_\nu = 6 \times 10^{23}\mathrm{m^{-3}}$, the TRICs (panel (a)) and TACs (panel (b)) of the MQD system with $x = 0.15 - 0.25 - 0.35 - 0.45$, $\eta = 0.35/a_0$, $T = 300\mathrm{K}$, $P = 3$ GPa and $\xi = 1$ kV/cm. The insets show the relevant energy differences and matrix elements, respectively, as $\Delta E = E_f - E_i$, $|M|^+ = |M_{if}|^2$, $|M|^x = |M_{ii} - M_{ff}|^2$.

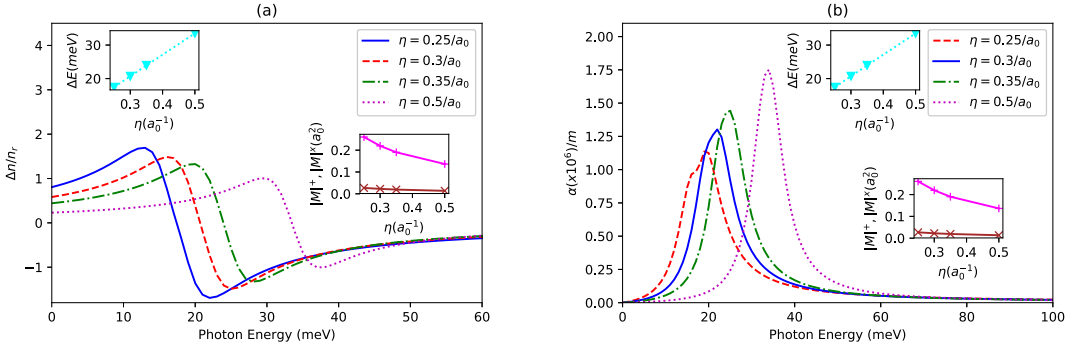

Fig. 7. When $I = 0.1 \times 10^{10}\mathrm{W/m^2}$ and $\sigma_\nu = 6 \times 10^{23}\mathrm{m^{-3}}$, the TRICs (panel (a)) and TACs (panel (b)) of the MQD system with $x = 0.15$, $\eta = (0.25 - 0.3 - 0.35 - 0.5)/a_0$, $T = 300\mathrm{K}$, $P = 3$ GPa and $\xi = 1$ kV/cm. The insets show the relevant energy differences and matrix elements, respectively, as $\Delta E = E_f - E_i$, $|M|^+ = |M_{if}|^2$, $|M|^x = |M_{ii} - M_{ff}|^2$.

is contrary character that of the TRICs, depending to the increment in electric field strength. As seen in Fig. 8b, the enhancement of the parameter ξ dramatically increases the TACs amplitudes. This is due to the predominance of the linear and nonlinear contributions of the absorption coefficients to each other, similar to the results of the other parameters.

The optical properties of the MQD have been also studied without the effect of the hydrogenic impurity atom at its center. It has been observed that the effective potential of the system changes very faintly in the absence of hydrogen impurity. For more detail, when the bound state energy levels are also probed, the hydrogenic impurity effect is again found to be very feeble, as expected. Therefore, it cannot be said that the hydrogenic impurity has an observable effect on optical properties in consideration of this quantum dot structure, and under related conditions. However, if impurities with larger atomic number can be employed instead of the

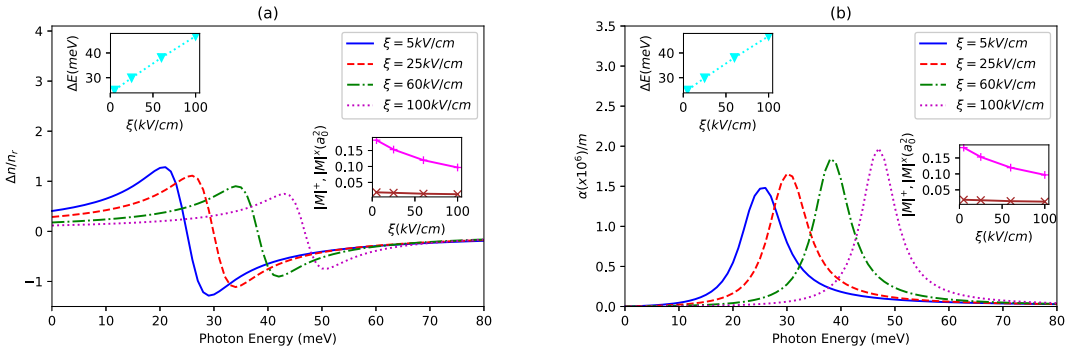

Fig. 8. When $I = 0.1 \times 10^{10}\mathrm{W/m^2}$ and $\sigma_v = 6 \times 10^{23}\mathrm{m^{-3}}$, the TRICs (panel (a)) and TACs (panel (b)) of the MQD system with $x = 0.15$, $\eta = 0.35/a_0$, $T = 300\mathrm{K}$, $P = 3$ GPa and $\xi = 5\text{–}25 - 60 - 100$ kV/cm. The insets show the relevant energy differences and matrix elements, respectively, as $\Delta E = E_f - E_i$, $|M|^+ = |M_{if}|^2$, $|M|^x = |M_{ii} - M_{ff}|^2$.

hydrogenic impurity, measurable quantities may result, which case is an expected case, because the Coulomb potential of the hydrogenic impurity is faint compared to other effects that make up the effective potential.

4. Conclusion

In this study, the TRICs and TACs of the MQD generated by the $In_xGa_{1-x}As/GaAs$ heterostructure, including the effects of the temperature, hydrostatic pressure, external electric field, and a centrally located donor impurity, have been theoretically probed. As well as the analysis of external parameters, it has been investigated that how to affect optical specifications structural parameters as *In*-concentration and MQD width. The notable results can be outlined as follows: i)The temperature has a slight weak influence on the TRICs and TACs. Because the response of the subband energies to temperature is too weak to be ignored. Therefore, the temperature is not an operational argument in optical sense either. ii)A decrement, resulting from augmenting hydrostatic pressure, in the TRICs and TACs amplitudes, and a redshift in relevant resonant frequencies are observed. The increment of the parameters x, η, and ξ are alternatives to each other in terms of their blue-shifting effects on the resonant frequencies. However, these parameters are also alternative to each other in terms of the TRICs and TACs amplitudes. In this manner, the hydrostatic pressure effect should be considered as a different external effect in terms of its effect on both the amplitude and resonant frequencies of the TRICs and TACs. iii) Increasing the optical intensity within special restrictions does not create instability in the system. Under the physical conditions in the present work, the optimal operating range of MQD for optical intensity has been determined, which is a notable gain for application studies. Here it should be pointed out that the ranges of all parameters in the work for optimal operations have been determined, and they are also achievable experimentally. This case has been very motivating for us in the sense that the present work overlaps with the implementation researches. As the MQD is a periodically repeating potential when considering a wider spatial limits, it can also be evaluated in the possible applications of multiple quantum wells, which is a remarkable point on the functionality of the MQD.

Declaration of competing interest

The authors declare that there is no conflict of interest.

Data availability

Data will be made available on request.

References

[1] K. Fu, Growth Dynamics of Semiconductor Nanostructures by MOCVD, Printed by Universitets service US AB, Stockholm, Sweden, 2009.
[2] M.J. Manfra, Molecular beam epitaxy of ultra-high-quality AlGaAs/GaAs heterostructures: enabling physics in low-dimensional electronic systems, Ann. Rev. Condensed Matter Phys. 5 (2014) 347.
[3] J. He, C.J. Reyner, B.L. Liang, K. Nunna, D.L. Huffaker, N. Pavarelli, K. Gradkowski, T.J. Ochalski, G. Huyet, V.G. Dorogan, Y.I. Mazur, G.J. Salamo, Band Alignment tailoring of $InAs_xSb_{1-x}GaAs$ quantum dots: control of type I to type II transition, Nano Lett. 10 (8) (2010) 3052.
[4] N.H. Jabarullah, Temperature dependence of quantum dots-in-well infrared photodetectors (QDIPs), Using Photoluminescence 54 (2019) 133.
[5] I. Lagraa, B. Soudini, H. Abid, S. Taleb, Study and optimization of structure InAs/InGaAs quantum dot in-a-well long-wave infrared photodetector, Optik 251 (2022), 168494.
[6] S. Kasap, P. Capper, Springer Handbook of Electronic and Photonic Materials, Springer, 2017.
[7] J. He, H.J. Krenner, C. Pryor, J.P. Zhang, Y. Wu, D.G. Allen, C.M. Morris, M.S. Sherwin, P.M. Petroff, Growth, structural, and optical properties of self-assembled (in,Ga)as quantum posts on GaAs, Nano Lett. 7 (2007) 802.
[8] H. Eisele, A. Lenz, R. Heitz, R. Timm, M. Dahne, Y. Temko, T. Suzuki, K. Jacobi, Change of InAs/GaAs quantum dot shape and composition during capping, J. Appl. Phys. 104 (2008), 124301.
[9] H. Marquez, L. Geelhaar, K. Jacob, Atomically resolved structure of InAs quantum dots, Appl. Phys. Lett. 78 (2001) 2309.

[10] M. Sabaeian, A. Khaledi-Nasab, Size-dependent intersubband optical properties of dome-shaped InAs/GaAs quantum dots with wetting layer, Appl. Opt. 51 (2012) 4176.
[11] J.H. Davies, The Physics of Low-Dimensional Semiconductors: an Introduction, 5.edition, Cambridge, USA, 1999.
[12] L. Jacak, Semiconductor quantum dots-towards a new generation of semiconductor devices, European Phys. J. 21 (2000) 487.
[13] F.M. Peeters, Magneto-optics in parabolic quantum dots, Phys. Rev. B 42 (1990) 1486. R.
[14] S. Mukhopadhyay, A. Chatterjee, Path-integral approach for electron–phonon interaction efects in harmonic quantum dots, Int. J. Mod. Phys. B 10 (1996) 2781.
[15] S. Mukhopadhyay, A. Chatterjee, Polaronic enhancement in the ground-state energy of an electron bound to a Coulomb impurity in a parabolic quantum dot, Phys. Rev. B 55 (1997) 9279.
[16] A. Boda, D.S. Kumar, I. Sankar, A. Chatterjee, Effect of electron–electron interaction on the magnetic moment and susceptibility of a parabolic GaAs quantum dot, J. Magn. Magn Mater. 418 (2016) 242.
[17] B.T. Miller, W. Hansen, S. Manus, R.J. Luyken, A. Lorke, J.P. Kotthaus, S. Huant, G. Medeiros-Ribeiro, P.M. Petroff, Few-electron ground states of charge-tunable self-assembled quantum dots, Phys. Rev. B 56 (1997) 6764.
[18] Z. Pachuau, B. Zoliana, D. Khating, P. Patra, R. Thapa, Application of Mathieu potential to photoemission from metals, Phys. Lett. 275 (2000) 459.
[19] G.H. Sun, C.Y. Chen, H. Taud, C. Yanez-Marquez, S.-H. Dong, Exact solutions of the 1d Schrödinger equation with the Mathieu potential, Phys. Lett. 384 (2020), 126480.
[20] S. Aghaei, A. Chenaghlou, N. Azadi, $1-D$ Dirac equation in the presence of the Mathieu potential, Europ. Phys. J. Plus 136 (2021) 749.
[21] T. Pearsall, $Ga_{0.47}In_{0.53}As$: a ternary semiconductor for photodetector applications, IEEE J. Quant. Electron. 16 (1980) 709.
[22] L.J. Mawst, H. Kim, G. Smith, W. Sun, N. Tansu, Strained-layer quantum well materials grown by MOCVD for diode laser application, Prog. Quant. Electron. 75 (2021), 100303.
[23] R.E. Nahory, M.A. Pollack, W.D. Johnston Jr., R.L. Barns, Band gap versus composition and demonstration of Vegard's law for $In_{1-x}Ga_xAs_yP_{1-y}$ lattice matched to InP, Appl. Phys. Lett. 33 (1978) 659.
[24] T. Pearsall, A $Ga_{0.47}In_{0.53}As$/InP heterophotodiode with reduced dark current, IEEE J. Quant. Electron. 17 (1981) 255.
[25] J. Faist, Quantum Cascade Laser, Oxford University Press, 2013.
[26] M. Tan, L. Ji, Y. Wu, P. Dai, Q. Wang, K. Li, T. Yu, Y. Yu, S. Lu, H. Yang, Investigation of InGaAs thermophotovoltaic cells under blackbody radiation, APEX 7 (2014), 096601.
[27] M. Di Dio, M. Lomascolo, A. Passaseo, C. Gerardi, C. Giannini, A. Quirini, L. Tapfer, Structural and optical studies of $In_xGa_{1-x}As$/GaAs multiple quantum wells, J. Appl. Phys. 80 (1996) 482.
[28] S. Martini, A.A. Quivy, E.C.F. da Silva, J.R. Leite, Real-time determination of the segregation strength of indium atoms in InGaAs layers grown by molecular-beam epitaxy, Appl. Phys. Lett. 81 (2002) 2863.
[29] H.P. Yu, C. Roberts, R. Murray, Influence of indium segregation on the emission from InGaAs/GaAs quantum wells, Appl. Phys. Lett. 66 (1995) 2253.
[30] L.F. Lester, S.D. Offsey, B.K. Ridley, W.J. Schaff, B.A. Foreman, L.F. Eastman, Comparison of the theoretical and experimental differential gain in strained layer InGaAs/GaAs quantum well lasers, Appl. Phys. Lett. 59 (1991) 1162.
[31] O. Mommadi, A. El Moussaouy, M. El Hadi, M. Chnafi, Y.M. Meziani, C.A. Duque, Stark shift and exciton binding energy in parabolic quantum dots: hydrostatic pressure, temperature, and electric field effects, Phil. Mag. 101 (2021) 753.
[32] C.S. Menoni, H.D. Hochheimer, I.L. Spain, High-pressure study of photoluminescence in indium phosphide at low temperature, Phys. Rev. B 33 (1986) 5896.
[33] N. Bouarissa, The effect of hydrostatic pressure on the electronic and optical properties of InP, Solid State Electron. 44 (2000) 2193.
[34] M. Chnafia, L. Belamkadema, O. Mommadia, R. Boussetta, M. El Hadia, A. El Moussaouya, F. Falyounia, J.A. Vinasco, D. Laroze, F. Mora-Rey, C.A. Duque, Hydrostatic pressure and temperature effects on spectrum of an off-center single dopant in a conical quantum dot with spherical edge, Superlattice. Microst. 159 (2021), 107052.
[35] S. Janati Edrissi, I. Zorkani, K. Rahmani, A. Mmadi, Y. Chrafih, A. Jorio, L. Leontie, The effect of hydrostatic pressure on the diamagnetic susceptibility of a magneto-donor in a GaAs cylindrical quantum dot, Optoelectron. Adv. Mater. Rapid Commun. 13 (2019) 111.
[36] S. Abdolhosseini, R. Kohandani, H. Kaatuzian, Analysis and investigation of temperature and hydrostatic pressure effects on optical characteristics of multiple quantum well slow light devices, Appl. Opt. 56 (2017) 7331.
[37] I. Karabulut, M.E. Mora-Ramos, C.A. Duque, Nonlinear optical rectification and optical absorption in GaAs–$Ga_{1-x}Al_xAs$ asymmetric double quantum wells: combined effects of applied electric and magnetic fields and hydrostatic pressure, J. Lumin. 131 (2011) 1502.
[38] J. You, Q. Zhao, Z. Zhang, The effect of temperature, hydrostatic pressure and magnetic field on the nonlinear optical properties of AlGaAs/GaAs semi-parabolic quantum well, Int. J. Mod. Phys. B 33 (2019), 1950325.
[39] X. Liu, L. Zou, C. Liu, Z. Zhang, J. Yuan, The nonlinear optical rectification and second harmonic generation in asymmetrical Gaussian potential quantum well: effects of hydrostatic pressure, temperature and magnetic field, Opt. Mater. 53 (2016) 218.
[40] M.J. Karimi, A. Keshavarz, Second harmonic generation in asymmetric double semi-parabolic quantum wells: effects of electric and magnetic fields, hydrostatic pressure and temperature, Phys. E Low-dimens. Syst. Nanostruct. 44 (2012) 1900.
[41] L. Aderras, A. Bah, E. Feddi, F. Dujardin, C.A. Duque, Stark-shift of impurity fundamental state in a lens shaped quantum dot, Phys. E Low-dimens. Syst. Nanostruct. 89 (2017) 119.
[42] L. Zhang, Z. Yu, W. Yao, Y. Liu, H. Ye, Linear and nonlinear optical properties of strained GaN/AlN quantum dots: effects of impurities, radii of QDs, and the incident optical intensity, Superlattice. Microst. 48 (2010) 434.
[43] L. Lu, W. Xie, Z. Shu, Combined effects of hydrostatic pressure and temperature on nonlinear properties of an exciton in a spherical quantum dot under the applied electric field, Phys. B Condens. Matter 406 (2011) 3735.
[44] B. Li, K.X. Guo, Z.L. Liu, Y.B. Zheng, Nonlinear optical rectification in parabolic quantum dots in the presence of electric and magnetic fields, Phys. Lett. 372 (2008) 1337.
[45] A. Oukerroum, E. Feddi, J. Bosch Bailach, J. Martinez-Pastor, F. Dujardin, E. Assaid, On the anomalous Stark effect in a thin disc-shaped quantum dot, J. Phys. Condens. Matter 22 (2010), 375301.
[46] E. Iqraoun, A. Sali, A. Rezzouk, E. Feddi, F. Dujardin, M.E. Mora-Ramos, C.A. Duque, Donor impurity-related photoionization cross section in GaAs cone-like quantum dots under applied electric field, Philos. Mag. A 97 (2017) 1445.
[47] M. Baira, B. Salem, N.A. Madhar, B. Ilahi, Intersubband optical nonlinearity of GeSn quantum dots under vertical electric field, Micromachines 10 (2019) 243.
[48] S.G. Nobandegani, M.J. Karimi, Effects of hydrogenic impurity and external fields on the optical absorption in a ring-shaped elliptical quantum dot, Opt. Mater. 82 (2018) 75.
[49] V. Yadav, M. Kria, J. El Hamdaoui, L.M. Perez, V. Prasad, M. El-Yadri, D. Laroze, E.M. Feddi, Quantum confined Stark effect on the linear and nonlinear optical properties of SiGe/Si semi oblate and prolate quantum dots grown in Si wetting layer, Nanomaterials 11 (2021) 1513.
[50] P. Zaithanzauva, B. Zoliana, D.T. Khating, P.K. Patra, R.K. Thapa, Application of Mathieu potential to photoemission from metals, Phys. Lett. 275 (2000) 459.
[51] S. Paul, J.B. Roy, P.K. Basu, Empirical expressions for the alloy composition and temperature dependence of the band gap and intrinsic carrier density in $Ga_xIn_{1-x}As$, J. Appl. Phys. 69 (2) (1991) 827.
[52] F. Ungan, M.K. Bahar, M.G. Barseghyan, L.M. Perez, D. Laroze, Effect of intense laser and electric fields on nonlinear optical properties of cylindrical quantum dot with Morse potential, Optik 236 (2021), 16662.
[53] S. Chaudhuri, Hydrogenic-impurity ground state in GaAs/$Ga_{1-x}Al_xAs$ multiple—quantum-well structures, Phys. Rev. B 28 (1983) 4480.
[54] S. Adachi, GaAs, AlAs, and AlxGa1xAs: material parameters for use in research and device applications, J. Appl. Phys. 58 (1985) R1.
[55] S. Paul, J.B. Roy, P.K. Basu, Empirical expressions for the alloy composition and temperature dependence of the band gap and intrinsic carrier density in $Ga_xIn_{1-x}As$, J. Appl. Phys. 69 (1991) 827.
[56] H.M. Baghramyan, M.G. Barseghyan, A.A. Kirakosyan, Effects of hydrostatic pressure and temperature on interband optical transitions in InAs/GaAs vertically coupled double quantum dots, J. Phys. Conf. 350 (2012), 012017.

[57] W.W. Chow, E.D. Jones, N.A. Modine, A.A. Allerman, S.R. Kurtz, Laser gain and threshold properties in compressive-strained and lattice-matched GaInNAs/GaAs quantum wells, Appl. Phys. Lett. 75 (1999) 2891.
[58] B.N. Datta, Numerical Linear Algebra and Applications, second ed., SIAM, Philadelphia, PA, USA, 2010.
[59] R.W. Boyd, Nonlinear Optics, third ed., Rochester, New York, 2007.
[60] G.B. Arfken, H.J. Weber, Mathematical Methods for Physicists, Academic, SanDiego, CA, 1995.
[61] K. Kılıç, M.K. Bahar, Optical response of plasma processed quantum dot under the external fields, Int. J. Quant. Chem. 121 (2021), e26564.